



Partial disordering and homogeneous melting in multicomponent systems



Guoying Zhang^a, Xue Fan^{b,*}, Qi Zhang^c, Qikai Li^d, Yuan Wu^a, Mo Li^{e,*}

^a State Key Laboratory for Advanced Metals and Materials, University of Science and Technology Beijing, Beijing 100083, China

^b Materials Genome Institute, Shanghai University, 99 Shangda Road, Shanghai 200444, China

^c Qian Xuesen Laboratory of Space Technology, China Academy of Space Technology, Beijing 100094, China

^d School of Chemistry, Tsinghua University, Beijing 100084, China

^e School of Materials Science and Engineering, Georgia Institute of Technology, Atlanta, Georgia 30332, United States

ARTICLE INFO

Article history:

Received 14 March 2022

Revised 16 August 2022

Accepted 16 August 2022

Available online 17 August 2022

Keywords:

melting

multicomponent alloy

self-diffusion

Lindemann criterion

high entropy alloy

ABSTRACT

Melting is a topological order-to-disorder transition where the crystal becomes disordered and turns into a liquid. In pure systems, melting is related to positional disordering only, whereas in multicomponent systems, it is affected also by the chemical component. Here, we report a first investigation of this important open issue in homogeneous melting in a five component model system, or high entropy alloy, with a particular focus on the atomic mechanisms. We show that melting proceeds with several stages dictated by the low melting point component: Partial disordering starts at a much lower temperature below the bulk melting point with the low melting point element executing an exceedingly large atomic displacement. Instead causing melting, the displaced element catalyzes the formation of mobile atomic chains and loops that still conform to the crystalline lattice. With increasing temperature, other elements gradually participate in these highly correlated atomic configurations, causing their growth and proliferation, and eventual formation of the liquid phase. The detailed atomic process provides a direct support for the recently proposed melting mechanisms involving the atomic chains and loops, rather than the Lindemann critical vibrational displacements.

© 2022 Acta Materialia Inc. Published by Elsevier Ltd. All rights reserved.

1. Introduction

Melting is a phase transition in which atoms or molecules are displaced at the melting point from their lattice positions and become topologically disordered. The atomic displacement has been considered vibrational in nature and is visible from the broadening of diffraction patterns in various scattering experiments. Therefore, one would think that melting is the direct result of the thermally agitated atomic vibrations. As put forward by Lindemann [1], when the atomic vibration amplitude becomes large enough to reach a critical value, atoms are displaced out of their lattice positions and become liquid. Extensive research in the past was carried out to establish the connection between the lattice vibration and the onset of melting via the critical Lindemann parameter (LP) that is assumed to be universal to crystals with the same type of structures [2–6]. The atomic displacement from the lattice positions is, therefore, used as the order parameter to measure the disordering; and

the critical LP is considered an identifier to distinguish whether or not an atom is in crystal or liquid state [7–10].

It is recognized recently [11–13], however, that during heating, atoms in crystals participate in not only vibrational but also other types of atomic movement that contribute significantly to the total atomic displacement: At temperatures far below melting point, atoms execute primarily vibrational motion, and at relatively high temperatures, diffusional motion sets in. The atoms participating in diffusion contribute significantly to the so-called mean-square displacement (MSD) which is the primary source of the atomic displacement identified and used in the Lindemann melting theory. Although the diffusional atomic displacements are in no way indicative of positional disordering as atoms move from lattice sites to lattice sites, they are still counted toward the total MSD in various atomic modeling [14–18] and erroneously, used in the Lindemann criterion to predict melting. This new finding brought up two questions that challenge our current understanding of melting. One is whether the Lindemann type of theories have properly identified and dealt with the order parameter, i.e. the MSD, in predicting melting, and the second is how the other types of atomic motions besides lattice vibration, are connected to melting.

* Corresponding authors.

E-mail addresses: fanxue2015@shu.edu.cn (X. Fan), mo.li@gatech.edu (M. Li).

In pure systems, we found that when heated toward melting point, vibration is the main source of displacement for atoms in the defect-free crystals when temperature is low. As the thermal agitation becomes larger at higher temperature, the atomic diffusion sets in with atoms hopping from their equilibrium lattice positions to the neighboring lattice sites. Those atoms participating in diffusion contributes significantly to the MSD. If one still includes this part of the displacement, the LP based on the total MSD would not follow the Lindemann universal criterion and thus, fails to predict melting [11–13]. Furthermore, rather than going randomly, a significant number of the diffusional atoms move together in a synchronous manner by forming chains, or even loops with the beginning of an atomic chain coinciding with the end. As temperature increases further toward melting point, the number of these so-called extended atomic configurations (EACs) increases, and melting occurs when these highly correlated configurations proliferate. This new atomic mechanism is fundamentally different from that of Lindemann where atomic movement is considered as vibrational, random, local, and independent.

So far, this new mechanism has been observed only in pure systems [11–13,19–21]. In mixtures or alloys with different components, we expect several complications to arise. The first is how the chemical components with different melting points, cohesive energies, and atomic sizes would change the atomic mechanisms of melting. One can imagine that the vibration amplitude of the alloy components with lower bonding energies, and lower melting points, would result in larger vibrational atomic MSD than those with higher bonding energies, and thus, make the atomic displacement heterogeneous. This scenario directly challenges the Lindemann's universal criterion for melting in which atomic displacements are homogeneous and only one universal critical MSD value is assumed. In other words, would the element with the largest MSD determine the onset of melting if melting is indeed as predicted by Lindemann criterion? If not, how do the different atomic displacements resulted from different components coordinate with each other to achieve the final melting?

How the chemical composition is coupled to the positional disorder underlying the topological phase transition is an important issue in understanding melting. It is well known that a large number of alloy systems exhibit various degrees of chemical segregation, or chemical inhomogeneity, when they are heated toward the solidus and liquidus line [22]. In addition to vibration, the segregating components certainly execute atomic displacement by diffusion, and the resulting atomic MSD becomes larger at higher temperature in the thermally activated process. Clearly, one cannot count this type of MSD as part of the contributions to the Lindemann critical value for predicting melting. However, the question of how exactly this type of atomic displacement caused by the chemical composition variation, which Lindemann did not anticipate, is coupled to the positional disordering for structural change in melting needs to be answered.

The next question is whether or not the new mechanism of melting with the EACs, or atomic chains and loops, discovered in one-component systems, would survive in alloy systems. Besides the atomic vibration, the formation of the highly correlated atomic motion as in EACs is another instance in converting the thermal energy to mechanical motion, or positional disordering, during melting. As temperature increases, the increasing anharmonicity and lattice distortion takes place. At the same time, formation of the EACs sets in. In mixtures or alloys with different chemical components, the different bonding strengths among the components may result in difference in atomic displacements, even at very low temperatures. In a random solid solution, for instance, one could imagine that the atomic displacements could become more random and easier for the low melting components. This *partial disordering* with certain chemical components may make the

vibration displacement more heterogeneous as compared to the pure systems. In addition, it could make the formation of the EACs more difficult because the different bonding energies and displacements may interrupt the correlated atomic motion in forming the EACs. These possible complications could jeopardize both the Lindemann's vibrational hypothesis and the EAC mechanisms. Therefore, we need to look into the fundamental question of how the chemical composition changes and how it contributes to the positional disordering for melting in alloy systems.

2. Methods

With these questions in mind, we carry out investigations in a multicomponent alloy. The system used is a single phase crystalline random solid solution with five components. To observe the atomic process of melting and the related atomic-level properties, we use molecular dynamics (MD) simulation. In the following, we describe the methods used in our work.

2.1. Sample preparation and simulation methods

The samples used in this work are made of five components that mimics the so-called Cantor high entropy alloy (HEA) with equimolar fraction of chemical components, $\text{Co}_{20}\text{Cr}_{20}\text{Fe}_{20}\text{Ni}_{20}\text{Mn}_{20}$, with an fcc structure [23,24]. We have three ways to build the initial structure. One is to put the five equimolar components randomly on an fcc lattice at 300 K and zero pressure in a cubic box with the periodic boundary conditions. Then we relax the sample for sufficiently long time until no energy or density drifting. The second is to take this sample and heat it to the temperature approximately 95% below the melting point at the heating rate of 10^{11} K/s; after holding the sample at this temperature for sufficiently long time we cool it down to 300 K. This heat treatment can not only reduce the residual stress and allow for structure relaxation, but also encourage certain degree of chemical equilibration that may not have a chance to achieve in the previous method. The third way is to heat the sample prepared with the first method above the melting point and then cool the liquid down to 300 K with the cooling rate of 10^{11} K/s. Upon freezing, the sample becomes polycrystals with grain boundaries and stacking faults and other crystal defects. The presence of these defects induces heterogeneous melting after the sample is heated again to high temperature. In this work, we do not use the samples prepared by this method. Nevertheless, the melting behaviors from the samples from the first two methods exhibit qualitatively the same trend. Therefore, we shall focus on the single crystal fcc random solutions prepared with these methods in this work.

In both the sample preparation and the subsequent melting, we use the classical MD simulation implemented via the large-scale atomic/molecular massively parallel simulator (LAMMPS) [25]. Heating, as well as cooling, is implemented with the isothermal-isobaric (NPT) ensemble MD method. The Noé-Hoover method [26,27] is used to control the temperature. The Newton equations of motion are solved numerically with a time step of 1 fs per step. For melting, we start with the samples at 300 K and then increase the temperature continuously with 10^{11} K/s heating rate until the crystal melts into a liquid. Different heating rates are tested that range from 10^{11} to 10^{13} K/s. No qualitative difference was found, except a slight change of melting temperature. In addition, to check further the heating rate effect, we tested isothermal heating, i.e., during heating we stop the temperature change and hold the sample at certain temperatures. In both the continuous and the isothermal heating, the atomic trajectories are collected for all atoms every 1 ps for analysis and calculation of structure and properties. The results from both heating schemes remain qualitatively the same. Hence, we shall primarily report the results from

the continuous heating. Since temperature T is linearly related to time t through the heating rate in the gradual heating, when applicable we plotted both the temperature and time at the bottom and top abscissa of the figures.

The atoms in the five-component model system interact with each other via the Lennard-Jones (LJ) potentials, $\phi_{\alpha\beta}(r_{ij}) = -4\epsilon_{\alpha\beta}(\sigma_{\alpha\beta}/r_{ij}^6 - \sigma_{\alpha\beta}/r_{ij}^{12})$, where i and j stand for i th and j th atom, α and β for the type of atoms, and $\epsilon_{\alpha\beta}$ and $\sigma_{\alpha\beta}$ are the LJ parameters. We use the available enthalpies of mixing and the cohesive energies of the pairs of atoms and the atomic sizes ($\sigma_{\alpha\beta}$ for $\alpha=\beta$) in the Cantor alloy made of Co, Cr, Fe, Ni, and Mn to fit the parameters [28]. For the cross interaction parameters of different types of atoms, $\sigma_{\alpha\beta}$ ($\alpha \neq \beta$), we take the average $\sigma_{\alpha\beta} = (\sigma_{\alpha\alpha} + \sigma_{\beta\beta})/2$. The cutoff distance is between the fifth and sixth nearest neighbors. The main motivation for using the LJ potential is to handle larger sample size needed to achieve good statistics for the multicomponent systems. As a comparison, we also tested many-body potentials such as the Modified Embedded Atom Method (MEAM) [29]. The sample statistics is relatively poor due to the much smaller system sizes limited by the MEAM potential, although qualitatively similar results are obtained. More details of these results are available from the authors or in the forthcoming separate publications [30].

The system size ranging from 32,000 to 500,000 atoms are used to test the size effect. As the thermal fluctuations are inversely proportional to the sample size, the larger fluctuation in the smaller systems results in slightly lower melting points. The difference, however, becomes negligible when the number of atoms approaches above 30 000 atoms. Since no significant size effects were found beyond this size, we shall report the results in this work from the samples with 32,000 atoms.

2.2. Characterization methods for disordering and melting

A. Mean square displacement (MSD) Firstly, we define the atomic square displacement $\Delta r_i(t)^2 = |\vec{r}_i(t) - \vec{r}_i(0)|^2$ for each atom i . The MSD is the distance square between the position $\vec{r}_i(t)$ at time t , or temperature T , and the position $\vec{r}_i(0)$ at temperature $T=300$ K and the initial time $t=0$. For a system at different time or temperature, the MSD is calculated by taking the average over the number of atoms, $\langle \Delta r^2 \rangle(t) = \frac{1}{N} \sum_{i=1}^N |\vec{r}_i(t) - \vec{r}_i(0)|^2$, where $\langle \dots \rangle$ stands for time average in the MD simulation and N can be the number of atoms for each component, or the entire sample. The choices for N gives the corresponding mean displacement for a specific component or the entire sample.

B. Lindemann parameter δ_L is defined as the ratio of the root-mean-square displacement, or $\langle \Delta r(t)^2 \rangle^{1/2}$, divided by the nearest neighbor distance, $\bar{r}_{nn}(t)$ at the same time t or temperature T . $\langle \Delta r(t)^2 \rangle^{1/2}$ and $\bar{r}_{nn}(t)$ can be obtained from the trajectories of the atoms in the MD simulation directly and used to monitor the onset of disordering or melting. If the MSD from each alloy component is calculated, we can obtain its corresponding partial Lindemann parameter.

C. Non-Gaussian parameter $\alpha_2 = \frac{3\langle \Delta r^4 \rangle}{5\langle \Delta r^2 \rangle^2} - 1$, where $\langle \Delta r^2 \rangle^2$ and $\langle \Delta r^4 \rangle$ can be obtained from the atomic displacement Δr discussed above. The Non-Gaussian parameter measures statistical heterogeneity of an underlying random variable. During heating of a crystal, the MSDs are homogeneous, or the displacement from each atom remains statistically the same by following a Gaussian distribution, hence the value of α_2 is zero. If certain atoms start to execute displacements larger than other atoms, or become non-Gaussian, such as partial disordering caused by certain alloy components, the value of α_2 starts to rise. Therefore,

from the change of α_2 , we can capture sensitively the starting temperature of disordering and how it is related to melting with respect to different components.

$$\textbf{D. Structure factor (SF)} S_i(k) = \langle \frac{1}{N^2} \left| \sum_{j=1}^N \exp(ik \bullet \vec{r}_{ij}) \right|^2 \rangle, \text{ where } \mathbf{k}$$

is the wave vector along the $\langle 111 \rangle$ directions in fcc structure, r_{ij} is the nearest neighbor pair distance centered at atom i , and j runs over all N nearest neighbors, and $N=12$ for the nearest neighbors. The SF defined this way is connected to the first diffraction peak with the wave vector \mathbf{k} from the most densely packed (111) planes. Its rise and fall indicates the degree of structure ordering. The value of the $S_i(k)$ is close to one in a perfect crystal and zero in liquid state.

E. Liquid atoms In order to identify the liquid phase formation in atomistic modeling, we need to label atoms that have the characteristics of a liquid. As influenced by Lindemann theory, the atomic MSD has been used for this purpose: When the MSD of an atom is larger than the value defined by the Lindemann critical parameter, the atom is called "liquid" or "liquid-like" [11–18,31–34]. Our work has shown that the atoms can have MSD larger than Lindemann critical parameter but are not liquid or liquid-like when they are engage in diffusional motion [11–13]. To label an atom correctly, one needs to use the SF since $S_i(k)$ measures the local atomic packing, rather than the atomic displacement. An atom is in "liquid" state if its SF value is below 0.2, or crystalline state if SF is larger. The critical value of 0.2 is chosen based on the mean $S(k)$ value at the crystal-liquid interface when the liquid of the sample coexists with the crystal at the equilibrium melting point [11–13,20].

F. Mobile atoms and atomic chains and loops To identify the correlated atomic movement and their configurations, we first need to define the mobile atoms that have their MSDs larger than the threshold value, $0.35r_{nn}$ for fcc, where r_{nn} is the nearest neighbor distance at a temperature. r_{nn} corresponds to the position of the valley between the first and the second neighbors in the corresponding crystals' radial distribution function (RDF). When the MSD is larger than this value, one can say that the atom has moved away from its lattice position and is "mobile". If two nearest atoms are moving away from their respective lattice positions simultaneously, they form the unit of the correlated atomic configuration [35–37]. For example, mobile atom i and j form a collective atom displacement if they are still each other's neighborhood, that is, $\min[|(r_i(\Delta t) - r_j(0))|, |(r_i(0) - r_j(\Delta t))|] < r^*$, where r^* is the threshold distance. By identifying all possible units of atoms that are moving together, we can map out the correlated atomic motions involved in the crystal. As shown below, these units take two forms, chain or loop.

3. Results

A. Homogeneous melting in multicomponent system

Fig. 1 summarizes the heating and final melting of the multicomponent system. As the system temperature increases, both the potential energy and the volume increase, and the density decreases. At the melting point ($T_m=1613$ K), all quantities show abrupt change, signaling a first order transition. Experimentally measured melting point for the Cantor alloy ranges roughly from 1500 K – 1650 K [38]. In our simulation the order-to-disorder transition is captured also by the local atomic packing via the coordination neighbor analysis (CNA) in the atomic configurations shown in the inset of Fig. 1: The orderly packed crystalline phase becomes gradually disordered as more and more local disorder shows up at higher temperature, and eventually becomes entirely disordered after melting.

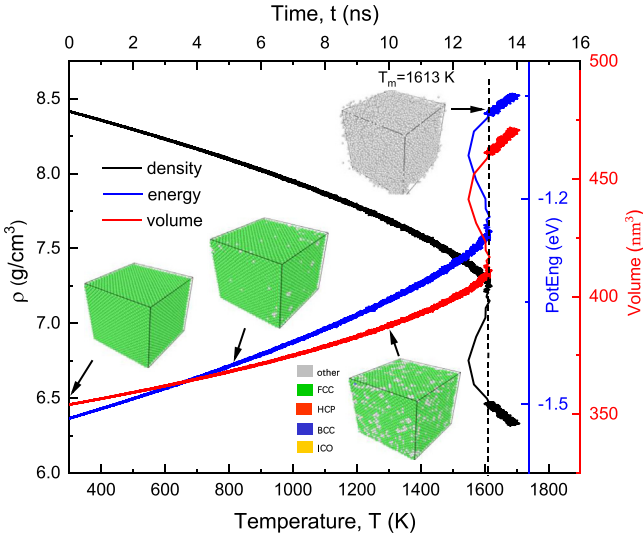


Fig. 1. The average potential energy, volume, and density of the sample versus temperature during continuous heating. The sample was prepared and relaxed at 300 K for 500 000 MD steps before being heated with the heating rate of 10^{11} K/s. The insets are the atomic configurations with the atoms marked by their local packing CNA index at 300 K, 800 K, 1300 K and 1613 K. The green color represents fcc local atomic packing and grey disordered packing. The top abscissa shows the heating time.

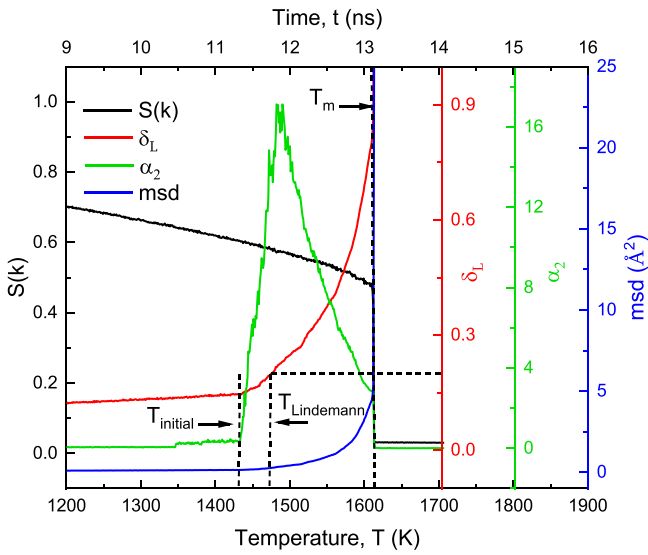


Fig. 2. The average MSD, Lindemann parameter δ_L , non-Gaussian parameter α_2 , and the structure factor SF versus temperature for the entire system. α_2 rises up abruptly at T_{initial} marked by a vertical dashed line. The predicted universal critical LP at 0.2 and the supposedly melting point $T_{\text{Lindemann}}$ predicted by Lindemann are marked with the horizontal and vertical dashed lines. The actual melting occurs at T_m . The top abscissa shows the heating time.

More detailed gauging of melting transition is shown in Fig. 2 where the MSD, Lindemann parameter δ_L , non-Gaussian parameter α_2 , and SF and their variations with increasing temperature are displayed. As in the pure systems [11–13], in the alloy the atomic displacement from their lattice positions at 300 K increases gradually with heating until about $T_{\text{initial}} = 1430$ K and then picks up rapidly before diverging at melting point. For this reason, we label this temperature as the initial disordering temperature, T_{initial} . The Lindemann parameter, however, exhibits a rather unusual behavior with an faster increasing trend starting at T_{initial} , well below the melting point. However, melting does not occur at the critical Lindemann critical value at 0.2 as predicted for fcc lattice when the

corresponding temperature $T_{\text{Lindemann}} = 1473$ K is approached. Melting occurs at a much higher value at $T_m = 1613$ K. At T_m , the LP value diverges. Note that this clear violation of Lindemann's criterion is not caused by overheating of the crystal because we observed the same results in isothermal case where the heating rate effect is absent.

The hint to the explanation of the above results lies in the behaviors of the non-Gaussian parameter α_2 in Fig. 2. At T_{initial} when δ_L suddenly rises up, α_2 also shows an abrupt increase from nearly zero to a large value. Since α_2 measures the heterogeneity of atomic displacements, the rapid rise indicates that there are certain atoms showing non-Gaussian displacements different from the rest of the atoms. The heterogeneous atomic displacements persist until melting where α_2 finally decays toward zero, or the displacement returns back to uniformity. During this temperature interval, the mean atomic displacements and δ_L clearly reach and pass beyond the Lindemann predicted critical value, and ironically the crystal structure still remain largely ordered as shown by the SF in Fig. 2. As we will elaborate in detail next, this finding is the centerpiece for revealing the melting mechanisms in the multicomponent systems.

B. Partial disordering of the low melting point component

The absence of melting in the multicomponent system at $T_{\text{Lindemann}}$ predicted by the critical Lindemann parameter is a clear and powerful example for rebuking the theory and its generality. The rapidly rising α_2 value at T_{initial} suggests that some sort of lattice disordering has already occurred at the much lower temperature that leads to the large MSD and δ_L . Nevertheless, the lattice structure still remains intact despite the Lindemann parameter already reaching and passing the critical value. One possibilities for the violation of Lindemann criterion is that some low melting point components in the alloy become disordered at low temperatures. Since the cohesive energy of Mn is the lowest among the alloy components (2.92 eV as compared to 4.10 eV of Cr [39], for example), its melting point is also the lowest, about 30% lower than that of Cr [40]. When heated, therefore, Mn atoms are expected to be displaced more easily due to the low cohesive energy and with a larger amplitude.

To verify this suspicion, we plot in Fig. 3(a) the MSD, Lindemann parameter δ_L , non-Gaussian parameter α_2 , and SF and their variation with increasing temperature for Mn. As a comparison, we also plot the mean values of each quantity averaged over the entire system which have been shown in Fig. 2. As shown below, the rest of the alloy components behave almost the same. Fig. 3(b) shows their δ_L and α_2 in comparison with those of Mn, so one can get a sense of how each component behaves with respect to Mn at the elevating temperature.

Fig. 3(a) and (b) show that Mn stands out always with much larger MSD and δ_L values at all temperatures compared to the mean values from the entire sample as well as those of the rest of the alloy components. For instance, at $T_{\text{Lindemann}}$, when the sample mean δ_L reaches the critical LP value of 0.2, the value for Mn is already 0.3. Or when δ_L value for Mn reaches 0.2 (while that for the rest of components is only slightly larger than 0.1 (Fig. 3(b)), the corresponding Lindemann temperature is about 1448 K, which is even lower than the system's $T_{\text{Lindemann}} = 1473$ K and far below the final melting point $T_m = 1613$ K. Once again, one can see that at this temperature the crystal structure still remains as indicated by the fairly large SF values for both Mn and the entire sample. Therefore, we can conclude that the Lindemann criterion does not apply to the multicomponent system, nor to the alloy component Mn, even though δ_L for Mn has already reached and past the critical LP values.

δ_L for Mn increases much faster and appears nearly diverging slightly below the melting point. The final melting occurs when δ_L 's for both Mn and the rest of the components reach values or-

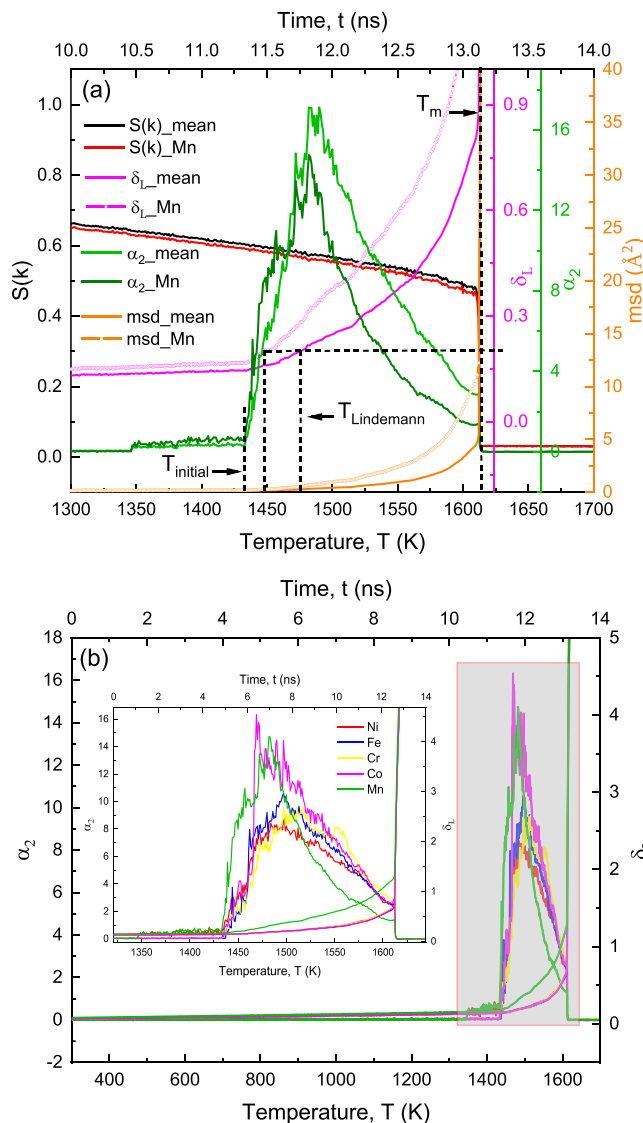


Fig. 3. (a) The mean MSD, Lindeman parameter δ_L , non-Gaussian parameter α_2 , and the structure factor SF versus temperature for the entire sample and Mn. The predicted universal critical LP value and the supposedly melting point predicted by Lindemann is marked with horizontal and vertical dashed lines. The Lindemann melting temperature corresponding to the critical LP value at 0.2 is at $T_{Lindemann} = 1473$ K for the system, but 1448 K for Mn. The actual melting occurs at T_m . The top abscissa shows the heating time. (b) The Lindeman parameter δ_L and non-Gaussian parameter α_2 versus temperature during heating for the alloy components. The top abscissa shows the heating time. The inset is a larger magnification of the curves between 1300 K and 1650 K.

ders of magnitude larger than the Lindemann's critical value. Since the mean quantities are calculated from all atoms, the much larger values for Mn atoms over the averaged values indicate that Mn is dominant from its partial disordering at low as well as high temperatures, whereas the rest of the four components behave more or less the same (Fig. 3(b)). This is evident since the rest of the components have nearly the same (large) values of the bonding strength and much higher melting points, and therefore, they contribute a much smaller fraction to those quantities.

This earlier-than-average positional disordering, or partial disordering, starting at low temperature for Mn is also captured accurately by α_2 which rises up abruptly at $T_{initial}$, while that of rest of the components has not changed yet (Fig. 3(b)). This difference in α_2 for different chemical components also indicates the sequence of the positional disordering in the multicomponent system dur-

ing heating that will be further illuminated in the formation of the EACs below.

C. Atom hopping and chemical concentration change for Mn

The MSD in Lindemann's theory to measure atomic position disorder is caused chiefly by vibrational motion. According to the theory, the vibrating atoms move away from their perfect lattice positions under thermal agitation; and when their amplitudes reach the critical Lindemann value, they lose their registry with the original lattice sites, and thus melting occurs. However, when temperature is high, atomic hopping sets in that can also contribute to the MSD. But because hopping in crystals happens with the atoms moving among lattice points, there will be no positional disordering caused by those atoms even though their MSDs can reach and pass the Lindemann critical value [11–13]. This can be seen clearly in Fig. 3 where the increasing MSDs have well past the Lindemann value, while the crystal lattice still remain ordered as measured by the large SF values.

Fig. 4(a) shows the distribution $P(\Delta r)$ of the mean atomic displacements Δr of all atoms at different temperatures and Fig. 4(b) for different components at 1550 K. One can see from Fig. 4(a) that at low temperatures below $T_{initial}$, the atomic MSD distribution is centered at values less than 0.25, meaning that the displacements are around each atom's lattice positions as they are executing vibrational motion. As temperature increases, the peak of the atomic displacement distribution becomes broader and its amplitude smaller as shown by the inset in Fig. 4(a).

As temperature approaches $T_{initial}$, there is a second peak emerging at the displacement about the first neighbor distance, r_{1nn} . The amplitude of the second peak plotted in the inset shows nearly zero value below $T_{initial}$ and picks up the value after. This means that the atomic displacement, or part of the MSD, can even reach the first neighbors, which is only possible when these atoms have actually hopped from their lattice positions to the first neighbor lattice sites. The hopping motion leads to large and heterogeneous MSDs that triggers the fast increase in the system's α_2 value (see the inset in Fig. 4(a)). At higher temperature, one can see more peaks showing up at the displacements corresponding to the second or third neighbor distances, meaning that the hopping motion has reached longer distances. Note that while the MSD keeps increasing from these diffusional motion as shown in Fig. 2 and 3, the crystal structure remains stable.

In Fig. 4(b) we plotted the atomic displacement distribution for each alloy component at 1550 K. Since significant long distance displacement occurs at this temperature, we can observe how each alloy component contribute to the hopping motion. Besides the general trends shown in Fig. 4(a) for the mean displacement distribution, one can clearly see that Mn differs from the rest of the components in this process: (1) It has larger vibration displacement amplitude as shown by the lower and more broad first peak width at low temperature as well as high temperature, and (2) it has much higher second, and even third peak heights, while the rest of the components have much smaller peak heights, indicating that more Mn atoms have already moved into those distant positions. In addition, other components show more or less the same distribution. The insets in Fig. 4(b) display the first and second peak heights, as well as the α_2 values for Mn at different temperatures. The rapid rise of α_2 correlates well with the emerging second peak height, meaning that some Mn atoms have started the excursion by hopping to the first neighbor positions when the critical LP is approached. Once again, there is no melting of the crystal structure.

Different from the rest of the components, the low melting point Mn atom starts hopping at lower temperature that contributes greatly to the overall MSD. This particular kinetic property can be confirmed by counting how many atoms from each components are in the first neighbors after their hopping. Fig. 5 shows

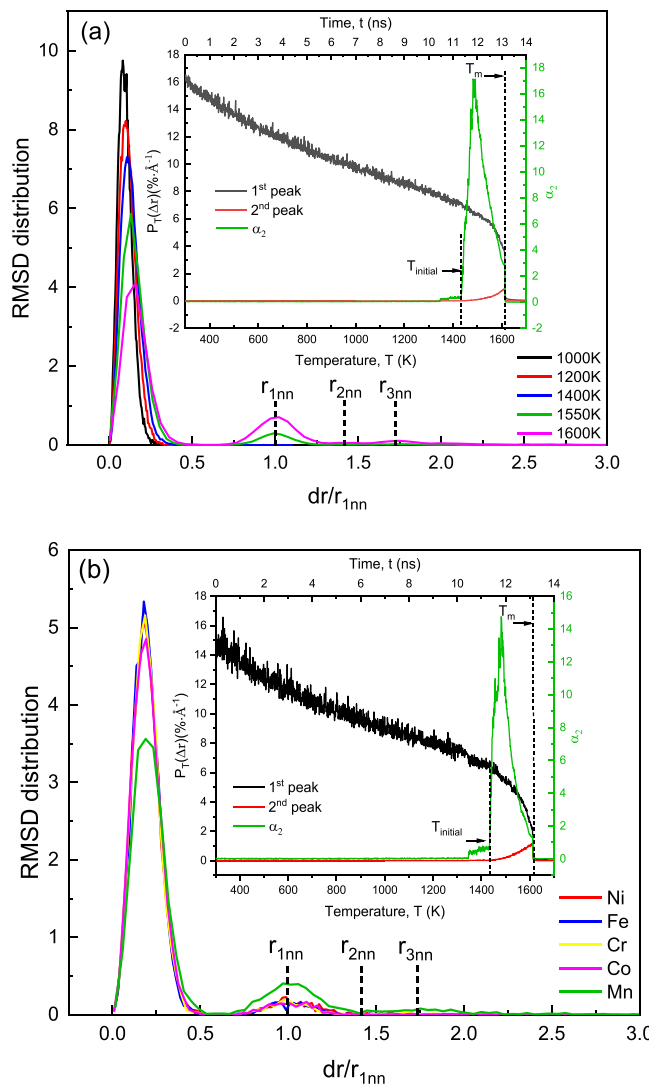


Fig. 4. (a) The distribution function of atomic displacement, $P(\Delta r)$, of the mean atomic displacement Δr of all atoms at different temperatures. Δr is normalized by the nearest neighbor distance, r_{1nn} . The first, second and third nearest neighbor distances are marked by r_{1nn} , r_{2nn} , and r_{3nn} . The inset is the height of the first and second peak in $P(\Delta r)$ and the non-Gaussian parameter α_2 versus temperature and heating time (top abscissa). The onset temperature $T_{initial}$ for non-zero α_2 and the melting point are marked. (b) The distribution function of atomic displacement, $P(\Delta r)$ of the mean atomic displacement Δr of all alloy components at 1550 K. Δr is normalized by the nearest neighbor distance, r_{1nn} . The inset is the height of the first and second peak in $P(\Delta r)$ and non-Gaussian parameter α_2 for Mn at different temperatures.

the fraction of the alloy components in the first neighbor sites at different temperatures. One can clearly see that at around $T_{initial}$, the only atoms hopping to the first neighbor sites are Mn with nearly 100% atomic fraction; as temperature increases, other types of atoms start to hop and move to the first neighbor sites, but the number of them are substantially smaller than Mn which maintains at about 40%, or twice the mean Mn concentration (20%) in the alloy, until 1560 K. At higher temperatures, the number of Mn atoms in the first neighbors declines slowly and other components increase. Finally, all components reach their alloy concentration at 20% at melting point, or in the liquid state. The enrichment of Mn among those hopped to their first neighbor sites reveals the preferred kinetic process by the low melting point element. The inset of Fig. 5 shows a typical atomic configuration of the atoms that have hopped to their first neighbors at 1480 K. The predominant number of Mn atoms in the first neighbor sites can be seen clearly.

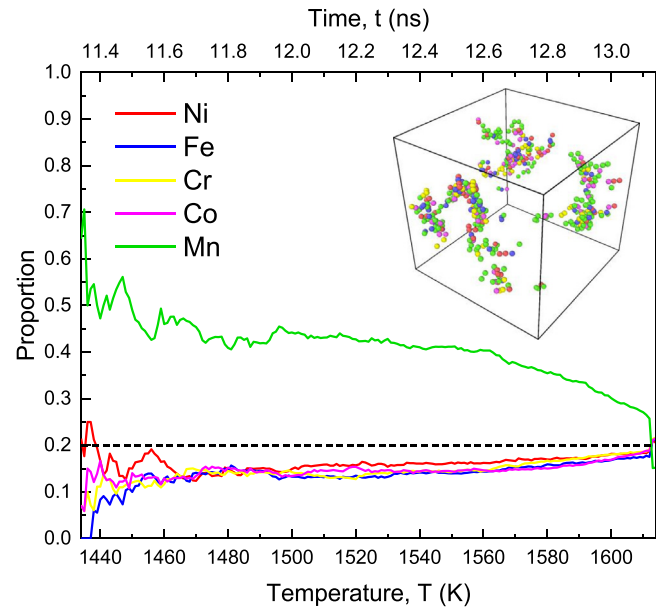


Fig. 5. The concentration of the alloy components at different temperatures that are in the first neighbor sites after the atoms hopped away from their original lattice sites. Hopping starts roughly around 1400 K, so we only plot the data above this temperature. The inset is a typical atomic configuration of the atoms that have hopped to their first neighbor sites at 1480 K. The color for the atoms in the inset matches that in the figure. The mean alloy concentration for all components is marked by a dashed line as a reference. The top abscissa shows the heating time.

As time goes on during heating, atoms hop to more distant neighbors. Fig. 4(b) shows that Mn atoms are not only the dominant one in hopping that take over the first neighbor sites, but also have higher fraction among the atoms hopping to the 2nd and 3rd neighbors. Clearly, this preferred hopping motion introduces local concentration change for Mn. However, as we show below, this alloy concentration change takes a special form confined by the one-dimensional atomic configuration of the EACs.

D. Formation of atomic chains and loops

The results presented above give a first detailed description of the atomic process of melting in multicomponent system that is highlighted by the presence of partial disordering and selective atom hopping by the low melting point component Mn that is joint later by other components at higher temperatures. Ironically, the disordering caused by Mn atoms does not cause melting as predicted from the Lindemann theory when its partial MSD reaches the critical LP (Fig. 3). Instead, these hopping atoms are organized in a highly correlated fashion to form the so-called extended atomic configurations in the form of chains and loops (Fig. 6). That is, when Mn atoms hopped from their lattice sites to the nearest neighbors, and later joined by other type of atoms, they appear to move in a synchronous way to form chain-like groups, which is the same as those observed in pure systems [11–13]. In the multicomponent system, the EACs are initiated by Mn atoms. This can be seen clearly already in the inset of Fig. 5 where the Mn atoms marked by green color appear to line up to form some sort of chains.

When other components join, the chains become multicomponent but always with a higher fraction of Mn atoms. In Fig. 6, we use pink circle to identify and mark the Mn atoms in different chains that are painted with different colors. Fig. 7 shows the concentration variation of the alloy components in the EACs at different temperatures. One can see that below 1560 K, the mean concentration of Mn atoms is in the range between 40–50% that is much larger than the mean alloy concentration at 20%; and the

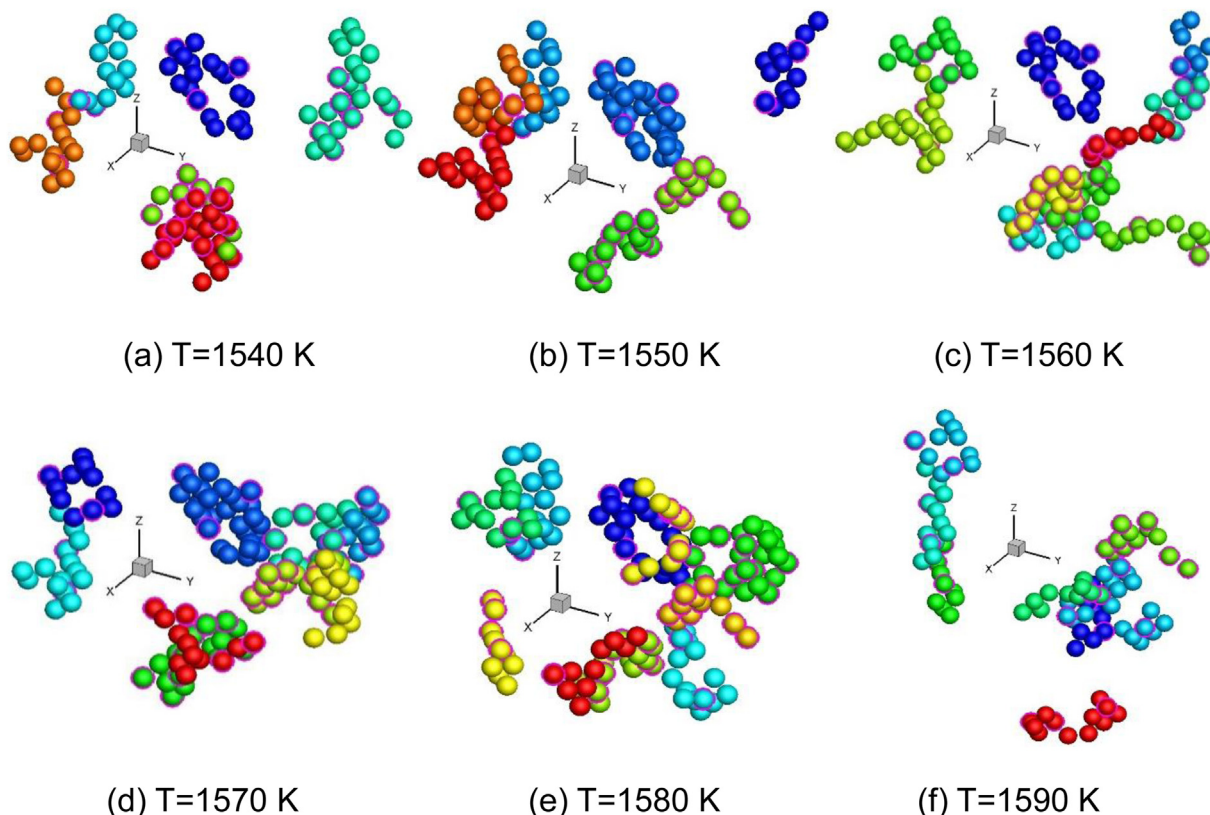


Fig. 6. The atomic configuration of the chains and loops at different temperatures slightly below the melting point. The atoms in each individual chain or loop is colored with the same color. Mn atoms in the chains or loops are identified by the pink circles around the atoms.

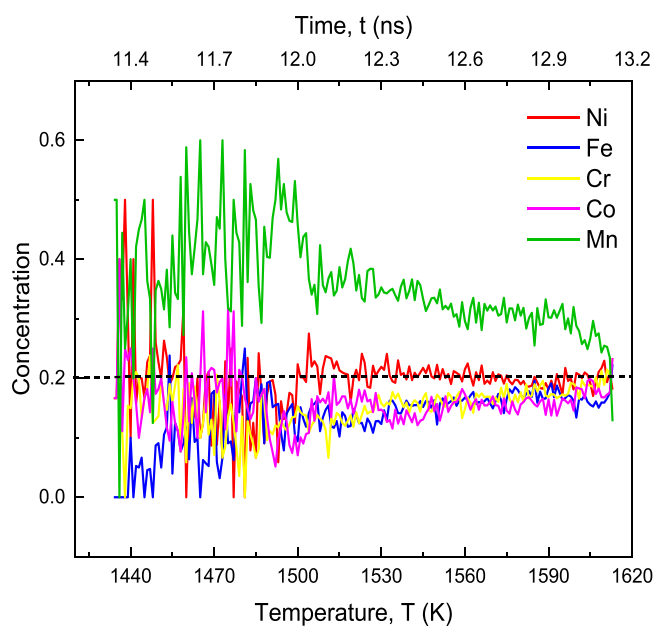


Fig. 7. The concentrations of different alloy components in the chains and loops at different temperature. The mean sample concentration for each alloy component is 0.2 that is marked by a black dashed line. The top abscissa shows the heating time.

concentrations of other components are below 20%. At about 1560 K, other components start to participate to the formation of the EACs as shown by a sudden increase in the atomic fractions of these atoms in the EACs. As a result, the relative concentration of Mn decreases. All concentrations approach the mean value at 20% at the melting point when the crystal becomes liquid.

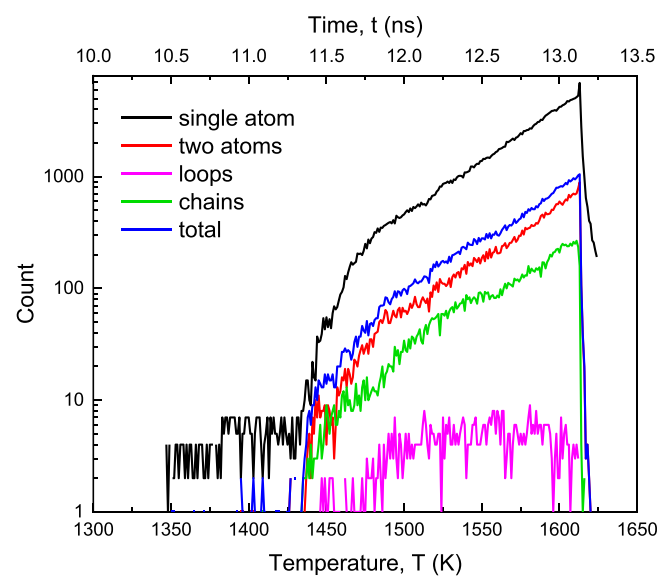


Fig. 8. The number of chains and loops in the multicomponent system at different temperatures during heating. For comparison, the single hopping atoms are also plotted. The top abscissa shows the heating time.

As more atoms are participating in forming the EACs at higher temperature, the number of the chains increases. As compared to the pure systems, the EACs in the multicomponent system do not have a significant number of loops; and in addition, there are substantial number of short chains consist of less than ten atoms. In Fig. 8, we plot the chains made of more than two synchronously moving atoms as well as those made of just two atoms as a com-

parison. As a reference, we also plot the number of single hopping atoms. One can see that as the length of the chains becomes longer, their numbers are smaller. The reason for the difficult to form long chains as seen in the pure systems is due primarily to the chemical disorder in the multicomponent system known for HEA [41–43]. The random distribution of the chemical components with different cohesive energies and atomic sizes introduces local chemical disorder that consequentially causes lattice distortion [44–45]. Both the chemical and lattice disorder in turn makes the long chain difficult to form. Or in other words, the chains formed are distorted too by the underlying lattice structure which is also affected by the differences in the chemical components. Finally, similar to what we found in pure systems, melting takes place when the EACs proliferate, or their total number approaches a critical value.

E. Homogeneous melting

As a first order transition, melting occurs within a narrow temperature window (see Fig. 1) around the melting point and undergoes a process of nucleation and growth of liquid phase. Fig. 9 shows the disordered regions made of atoms marked by SF values between the temperature ranges from 1604 K to 1606 K, just slightly before melting point at 1613 K. When the SF value of atoms is less than or equal to 0.2, they are in liquid state. The validity of this threshold value is confirmed by the observation of the equilibrium liquid-crystal interface at the melting point where the SF across the interface from the crystal to the liquid phase side has the midpoint at 0.2 [20]. One can see in Fig. 9 that within this short temperature range, the disordered regions form with the size ranging from a few atoms to hundreds of atoms. In addition, these regions appear and disappear dynamically. The smaller disordered regions have higher likelihood to disappear, while the larger ones survive (see the red region on the top right corner in Fig. 9). Approaching the melting point, only a few large regions with the liquid atoms remain and grow further that eventually consume the entire system.

As mentioned in the previous sections, Mn atoms are the facilitator for the initial partial disordering with the largest atomic displacements and also the formation of the EACs. Therefore, Mn atom becomes naturally a “tracer” so we can use it to identify the connection of the disordered regions and the EACs during heating. In Fig. 9 we identified those Mn with thick white circles around them that are in the liquid phase during the nucleation and growth. One can see that indeed, the formation of the disordered regions or liquid phase is closely associated with enriched Mn atoms and through the EACs.

4. Discussions and conclusions

Despite the extensive research performed over a century, the detailed atomic mechanisms of melting remain unclear and often controversial. Specifically, how atoms (dis-)organize themselves during heating and finally melt is still one of the mysteries in science. The simplistic explanations [46–48] such as the Lindemann theory describe melting as caused by a critical atomic displacement beyond which the atoms cannot return to or register with their original lattice positions. The defect-induced melting theories [49–50], on the other hand, give more details about how the atoms lose their order via formation of crystal defects which are naturally disordered to begin with. Hence, melting is described as a production of crystal defects. For homogeneous melting in perfect crystals where no defects or other structural heterogeneity are present to induce melting, the fundamental questions of how atoms lose their order on their crystal lattice sites is still unresolved.

Our previous work reveals that in addition to the independent and random atomic displacement in vibration as described by Lindemann, atoms in defect-free crystals during heating can also

move in highly organized ways through hopping together and form atomic chains and loops [11–13]. Melting occurs when these EACs become populated. The motion of different chains or loops interact and exert forces on each other that not only disrupt the highly organized atomic displacements but also cause the positional disorder for atoms on the crystal lattices. In the multicomponent system, we expect the same mechanism to manifest with much clarity because the formation of the EACs are characterized predominantly by the low-melting-point component like Mn. This is like putting a marker on the atoms so one can see how they initiate and facilitate the formation of EACs and melting by following those atoms through Mn. Our results in the multicomponent system show that melting is a positional disordering process with the atomic displacements made of both the vibrational and hopping motion. The simplicit description of using only the vibrational displacement at a universal threshold clearly misses the latter, especially for homogeneous melting when no heterogeneous nucleation mechanisms are available. The hopping motion at relatively high temperature introduces atomic displacement that does not cause topological disorder. However, when the correlated atomic motion in the form of chains and loops increases and proliferates, melting occurs. This is clearly caused by the position disorder of displaced atoms from both the EACs and their interactions, as well as the atoms surrounding them.

In multicomponent systems, addition of alloy components brings in differences in atomic bonding as well as atomic size. These additional factors absent in pure systems influence atomic displacements in not only the magnitude but also the EACs. The low-melting-point component such as Mn has large displacement amplitude in both vibration and hopping motion, and also prone to move collectively to form atomic chains and loops. The partial disordering caused by the chemical splices is the leading factor in initiating and formation of the liquid phase. And also because of its active role in facilitating the atomic vibrational as well as hopping motion, Mn is natural enriched in the EACs and disordered regions that eventually form liquid. This discovery may point to an experimental approach to detect liquid phase formation during melting by singling out the key chemical component such as Mn. This natural chemical marker may reveal the long-sought-after atomic mechanisms of homogeneous melting.

Since the samples used in this work is defect free and also subject to the periodic boundary conditions, certain superheating is expected, i.e., the melting point is higher than that obtained from equilibrium melting of crystals with the presence of crystal-liquid interfaces [51–52]. Another reason for superheating is due to heating rate. High heating rate is known to push the melting point higher in first order phase transitions. In multicomponent systems, we found that the heating rate effect is much weaker when we compare the melting point obtained from the fast heating with that from isothermal heating. The main reason is the presence of the chemical disorder, or specifically, the low-melting-point component Mn. The Mn induced partial disordering occurred internally greatly reduces the kinetic barrier for liquid phase formation and thus superheating.

The main feature of the multicomponent system is the coupling between the chemical disorder, i.e. the random distribution of different alloy components on lattices, and the structure disordering. We learned from this work that the structure or positional disordering caused by the chemical effect is reflected in the following aspects: (1) larger vibrational atomic displacement due to the weakly bonded Mn that occurs at much lower temperature, (2) preferred participation in hopping motion that leads directly to the formation of the EACs, and (3) facilitating formation of liquid phase with local and partial disorder and chemical enrichment in the disordered regions. These aspects absent in pure systems should re-

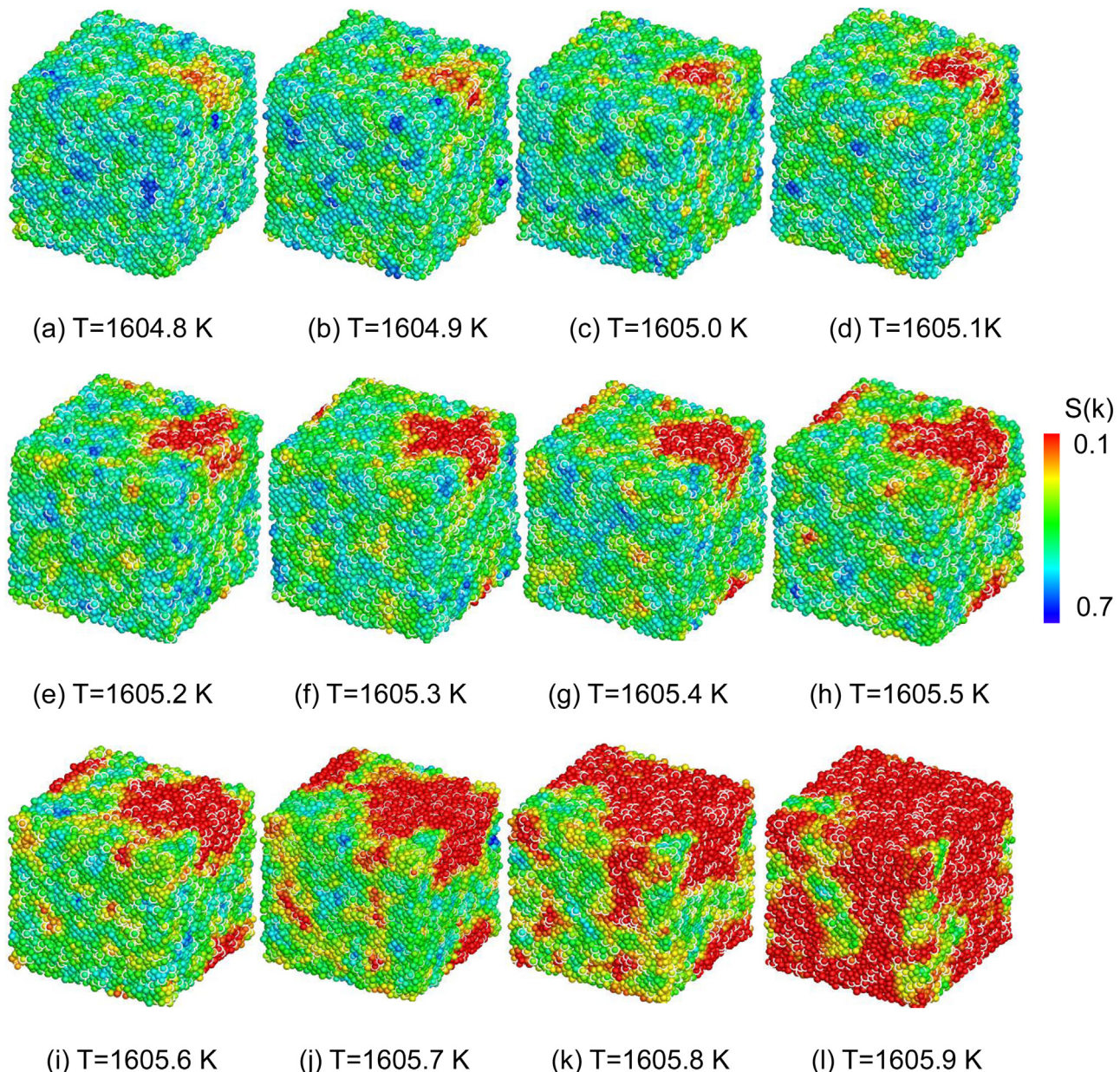


Fig. 9. The atomic configurations of the atoms marked by the structure factor at different temperatures close to the melting point. The warm color represents the atoms with severe disorder. The liquid atoms are marked as red with the SF value less than 0.2. The atom with the white circle is Mn.

main universal for other mixed systems as long as the differences exist among the alloy components.

The first order phase transition such as crystallization from liquid to crystal has been extensively and often successfully described by theoretical models. However, the first order melting transition has not been the case. Unlike crystallization where the ordered crystalline embryos are well described by structural order and the crystal-liquid interface, the formation of the liquid nuclei and their thermodynamic barrier in melting depends largely on the detailed understanding of the underlying atomic mechanisms and physical entities or disordering. High temperature and the omnipresent menace of the heterogeneous nucleation makes it highly challenging to obtain reliable results. Our theoretical work opens a small window that shows a different picture of melting transition. We hope our results would

stimulate more interests in exploring this fascinating unsolved problem.

Declaration of Competing Interest

The authors declare no conflict of interest.

Acknowledgment

G.Y.Z. would like to thank the graduate research support provided by the State Key Laboratory for Advanced Metals and Materials, University of Science and Technology Beijing and also the internship provided by the Qian Xuesen Laboratory of Space Technology, China Academy of Space Technology.

References

- [1] V.F.A. Lindemann, Über die Berechnung molekularer Eigenfrequenzen, *Phys. Z.* 11 (1910) 609–612.
- [2] J.E. Lennard-Jones, A.F. Devonshire, Critical and co-operative phenomena. IV. A theory of disorder in solids and liquids and the process of melting, *Proc. Roy. Soc. (Lond.) A* 170 (1939) 464.
- [3] J.J. Gilvarry, The Lindemann and Grüneisen laws, *Phys. Rev.* 102 (1956) 308–316.
- [4] J.-P. Hansen, Phase Transition of the Lennard-Jones System. II. High-temperature limit, *Phys. Rev. A* 2 (1970) 221–230.
- [5] R.W. Cahn, Crystal defects and melting, *Nature* 273 (1978) 491–492.
- [6] F.H. Stillinger, T.A. Weber, Lindemann melting criterion and the Gaussian core model, *Phys. Rev. B* 22 (1980) 3790–3794.
- [7] S.A. Cho, Role of lattice structure on the Lindemann fusion theory of metal, *J. Phys. F Met. Phys.* 12 (1982).
- [8] J. Daeges, H. Gleiter, J.H. Perepezko, Superheating of metal crystals, *Phys. Lett. A* 119 (1986) 4.
- [9] S.-N. Luo, A. Strachan, D.C. Swift, Vibrational density of states and Lindemann melting law, *J. Chem. Phys.* 122 (2005) 194709.
- [10] Q.S. Mei, K. Lu, Melting and superheating of crystalline solids: from bulk to nano-crystals, *Prog. Mater. Sci.* 52 (2007) 1175–1262.
- [11] X.M. Bai, M. Li, Ring-diffusion mediated homogeneous melting in the superheating regime, *Phys. Rev. B* 77 (2008) 134109.
- [12] H. Zhang, M. Khalkhal, Q. Liu, J.F. Douglas, String-like cooperative motion in homogeneous melting, *J. Chem. Phys.* 138 (2013) 12A538.
- [13] X. Fan, D. Pan, M. Li, Melting of bcc crystal Ta without the Lindemann criterion, *J. Phys. Condens. Matt.* 31 (2019) 095402.
- [14] H.a.M.M. Hakkinen, Computer simulation of disordering and premelting of low-index faces of copper, *Phys. Rev. B* 46 (1992) 1725–1742.
- [15] W. Theis, K. Horn, Surface premelting in Al(110) observed by core-level photoemission, *Phys. Rev. B Condens. Matter* 51 (1995) 7157–7159.
- [16] H. Kleinert, Y. Jiang, Defect melting models for cubic lattices and universal laws for melting temperatures, *Phys. Lett. A* 313 (2003) 152–157.
- [17] F.L. Tang, X.G. Cheng, W.J. Lu, W.Y. Yu, Premelting of Al nonperfect (111) surface, *Physica B: Condensed Matter* 405 (2010) 1248–1252.
- [18] R. Kojima, M. Susa, Surface melting of copper with (100), (110), and (111) orientations in terms of molecular dynamics simulation, *High Temperatures – High Pressures* 34 (2002) 639.
- [19] S. Sarkar, C. Jana, B. Bagchi, Breakdown of universal Lindemann criterion in the melting of Lennard-Jones polydisperse solids, *J. Chem. Sci.* 129 (2017) 833–840.
- [20] X. Fan, D. Pan, M. Li, Rethinking Lindemann criterion: A molecular dynamics simulation of surface mediated melting, *Acta Mater.* 193 (2020) 280–290.
- [21] C. Chakravarty, P.G. Debenedetti, F.H. Stillinger, Lindemann measures for the solid-liquid phase transition, *J. Chem. Phys.* 126 (2007) 204508.
- [22] D. Karlsson, A. Marshal, F. Johansson, M. Schusky, M. Sahlberg, J.M. Schneider, U. Jansson, Elemental segregation in an AlCoCrFeNi high-entropy alloy – A comparison between selective laser melting and induction melting, *J. Alloys and Comp.* 784 (2019) 195–203.
- [23] J.W. Yeh, S.K. Chen, S.J. Lin, J.Y. Gan, T.S.H. Chin, T.T. Shun, C.H.H. Tsau, S.H.Y. Chang, Nanostructured High-Entropy alloys with multiple principal elements: novel alloy design concepts and outcomes, *Adv. Eng. Mater.* 6 (2004) 299–303.
- [24] B. Cantor, I.T.H. Chang, P. Knight, A.J.B. Vincent, Microstructural development in equiatomic multicomponent alloys, *Mater. Sci. Eng. A* 375–377 (2004) 213–218.
- [25] S. Plimpton, Fast parallel algorithms for short-range molecular dynamics, *J. Comput. Phys.* 117 (1995) 1–19.
- [26] S. Nosé, A unified formulation of the constant temperature molecular dynamics methods, *J. Chem. Phys.* 81 (1984) 511–519.
- [27] W.G. Hoover, Canonical dynamics: Equilibrium phase-space distributions, *Phys. Rev. A* 31 (1985) 1695–1697.
- [28] W. Kob, H.C. Andersen, Testing mode-coupling theory for a supercooled binary Lennard-Jones mixture-The Van Hove correlation-function, *Phys. Rev. E* 51 (1995) 4626–4641.
- [29] W.M. Choi, Y.H. Jo, S.S. Sohn, S. Lee, B.J. Lee, Understanding the physical metallurgy of the CoCrFeMnNi high-entropy alloy: an atomistic simulation study, *NPJ Comput. Mater.* (2018).
- [30] G.Y. Zhang, M. Li. Unpublished.
- [31] H. Zhang, P. Kalvapalle, J.F. Douglas, String-Like Collective Atomic Motion in the Melting and Freezing of Nanoparticles, *J. Phys. Chem. B* 115 (2011) 14068–14076.
- [32] H. Zhang, D.J. Srolovitz, J.F. Douglas, J.A. Warren, Characterization of atomic motion governing grain boundary migration, *Phys. Rev. B* 74 (2006) 115404.
- [33] X. Fan, X.H. Chen, D. Pan, Y. Liu, P. Liu, M. Li, Localization and delocalization of surface disordering in surface mediated melting, *Phys. Rev. B* 104 (2021) 134204.
- [34] V.G. Chudinov, R.M.J. Cotterill, V.V. Andreev, Possible Mechanism for the Solid-Liquid Phase Transition in HCP and BCC Structure, *Phys. Stat. Sol.* 122 (1990) 187.
- [35] C. Donati, J.F. Douglas, W. Kob, S.J. Plimpton, P.H. Poole, S.C. Glotzer, Stringlike Cooperative Motion in a Supercooled Liquid, *Phys. Rev. Lett.* 80 (1998) 2338.
- [36] W. Kob, C. Donati, S.J. Plimpton, P.H. Poole, S.C. Glotzer, Dynamical heterogeneities in a supercooled Lennard-Jones liquid, *Phys. Rev. Lett.* 79 (1997) 2827.
- [37] C. Donati, S.C. Glotzer, S.J. Plimpton, Spatial correlations of mobility and immobility in a glass-forming Lennard-Jones liquid, *Phys. Rev. E* 60 (1999) 3107.
- [38] L.R. Owen, E.J. Pickering, H.Y. Playford, H.J. Stone, M.F. Tucker, N.G. Jones, An assessment of the lattice strain in the CrMnFeCoNi high entropy alloy, *Acta Mater.* 122 (2017) 11–18. E.J. Pickering, R. Mu~noz-Moreno, H.J. Stone, N.G. Jones, Precipitation in the equiatomic high-entropy alloy CrMnFeCoNi, *Scr. Mater.* 113 (2016) 106; K.-Y. Tsai, M.-H. Tsai, J.-W. Yeh, Sluggish diffusion in Co-Cr-Fe-Mn-Ni high-entropy alloys, *Acta Mater.* 61 (2013) 4887–4897; M. Vaidya, S. Trubel, B.S. Murty, G. Wilde, S.V. Divinski, Ni tracer diffusion in CoCrFeNi and CoCrFeMnNi high entropy alloys, *J. Alloys Compd.* 688 (2016) 994–1001; M. Laurent-Brocq, A. Akhatova, L. Perrière, S. Chebini, X. Sauvage, E. Leroy, Y. Champion, Insights into the phase diagram of the CrMnFeCoNi high entropy alloy, *Acta Materialia*, 88 (2015) 355–365.
- [39] C. Kittel, *Introduction to Solid State Physics*, 8th ed., John Wiley & Sons, 2004.
- [40] B.-J. Lee, M.I. Baskes, H. Kim, Y.K. Cho, Second nearest-neighbor modified embedded atom method potentials for bcc transition metals, *Phys. Rev. B* 64 (2001) 184102.
- [41] S.L. Thomas, S. Patala, Vacancy diffusion in multi-principal element alloys: The role of chemical disorder in the ordered lattice, *Acta Mater.* 196 (2020) 144–153.
- [42] J.W. Yeh, S.J. Lin, T.S. Chin, J.Y. Gan, S.K. Chen, T.T. Shun, Formation of simple crystal structures in Cu-Co-Ni-Cr-Al-Fe-Ti-V alloys with multiprincipal metallic elements, *Metall. Mater. Trans. A* 35 (2004) 2533–2536.
- [43] D.B. Miracle, O.N. Senkov, A critical review of high entropy alloys and related concepts, *Acta Mater.* 122 (2017) 448–511.
- [44] L.R. Owen, E.J. Pickering, H.Y. Playford, H.J. Stone, M.G. Tucker, N.G. Jones, An assessment of the lattice strain in the CrMnFeCoNi high-entropy alloy, *Acta Mater.* 122 (2017) 11–18.
- [45] H.Q. Song, F.Y. Tian, Q.M. Hu, L. Vitos, Y.D. Wang, J. Shen, N.X. Chen, Local lattice distortion in high-entropy alloys, *Phys. Rev. Mater.* (2017) 023404.
- [46] A.V. Granato, D.M. Jancich, V.A. Kholik, Melting, thermal expansion, and the Lindemann rule for elemental substances, *Appl. Phys. Lett.* 97 (2010) 171911.
- [47] A.C. Lawson, Physics of the Lindemann melting rule, *Philos. Mag.* 89 (2009) 1757–1770.
- [48] J.N. Shapiro, Lindemann Law and Lattice Dynamics, *Phys. Rew. B.* 1 (1970) 3982–3989.
- [49] A.M. Alsayed, M.F. Islam, J. Zhang, P.J. Collings, A.G. Yodh, Premelting at Defects Within Bulk Colloidal Crystals, *Science* 309 (2005) 1207–1210.
- [50] A. Samanta, M.E. Tuckerman, T.Q. Yu, W.N. E, Microscopic mechanisms of equilibrium melting of a solid, *Science* 346 (2014) 729–732.
- [51] J.R. Morris, C.Z. Wang, K.M. Ho, C.T. Chan, Melting line of aluminum from simulations of coexisting phases, *Phys. Rev. B* 49 (1994) 3109–3115.
- [52] J.R. Morris, X. Song, The melting lines of model systems calculated from coexistence simulations, *J. Chem. Phys.* 116 (2002) 9352–9358.